Inorg. Chem. **2002**, *41*, 4763–4769

Metallic Conductivity and Ferromagnetic Interaction of Iron(III) d Spins in the Needle Crystals of (Ethylenedithiotetrathiafulvalenoquinone-1,3-dithiolemethide)$_2$·FeBr$_4$ Salt

Takuya Matsumoto,[†] Tsuyoshi Kominami,[†] Kazumasa Ueda,[†] Toyonari Sugimoto,*[,†,▽] Toshiji Tada,[†] Satoru Noguchi,[‡] Harukazu Yoshino,[§] Keizo Murata,[§] Motoo Shiro,[∥] Ei-ichi Negishi,[⊥] Naoki Toyota,[⊥,▽] Satoshi Endo,[#] and Kazuko Takahashi[▽]

Research Institute for Advanced Science and Technology, Osaka Prefecture University, Osaka 599-8570, Japan, Graduate School of Engineering, Osaka Prefecture University, Osaka 599-8531, Japan, Graduate School of Science, Osaka City University, Osaka 558-8585, Japan, Rigaku Corporation, Tokyo 196-8666, Japan, Graduate School of Science, Tohoku University, Sendai 980-8578, Japan, Center for Low-Temperature Science, Tohoku University, Sendai 980-8577, Japan, and Center for Interdisciplinary Research, Tohoku University, Sendai 980-8577, Japan

Received February 19, 2002

The 2:1 charge-transfer (CT) salts (**1**$_2$·FeBr$_4$ and **1**$_2$·GaBr$_4$) of ethylenedithiotetrathiafulvalenoquinone-1,3-dithiolemethide (**1**) with FeBr$_4^-$ and GaBr$_4^-$ counteranions were obtained as needle crystals, whose structures are almost the same as each other. The **1** molecules form a one dimensionally stacked column with alternation of their molecular axis direction, while the counteranions are aligned in parallel with the **1**-stacked columns with the direction of their distorted-tetrahedral geometry maintained. The room-temperature electrical conductivities measured on the single crystals of **1**$_2$·FeBr$_4$ and **1**$_2$·GaBr$_4$ were 4.6 and 2.1 S cm^{-1}, respectively. From the temperature dependences of their electrical conductivities in both cases the electrical conducting properties were metallic between ca. 170 and 300 K, but below ca. 170 K converted to be semiconducting and continued till 5 K, although the activation energies are very small (4–10 meV). For **1**$_2$·FeBr$_4$ very weak and antiferromagnetic interaction occurred between the d spins of FeBr$_4^-$ ions in the temperature range of ca. 1–300 K. However, below ca. 15 K the ferromagnetic interaction was reversely preferential possibly by participation of the π spin of **1**.

Introduction

Current interest continues to be directed toward molecular/organic magnetic conductors, in which conducting π electrons and local π or d spins are expected to significantly interact with each other so as to produce unusual electrical conducting and/or magnetic properties.[1] Especially, a great deal of progress has been made so far in several charge-transfer (CT) salts of π donor molecules with magnetic-metal counteranions, as is obvious from most epoch-making examples of paramagnetic superconductors based on β'' -[bis(ethylenedithio)tetrathiafulvalene]$_4$·[(H$_2$O)M(C$_2$O$_3$)]·PhCN (bis(ethylenedithio)tetrathiafulvalene = BEDT-TTF; M = Fe, Cr),[2,3] an antiferromagnetic superconductor based on κ-[bis(ethylenedithio)tetraselenafulvalene]$_2$·FeBr$_4$ (bis(ethylenedithio)tetraselenafulvalene = BETS),[4,5] an antiferromagnetic metal based on (3,4-ethylenedithio-3′,4′- dimethyl-2,5-dithia-

* Author to whom correspondence should be addressed. E-mail: toyonari@riast.osakafu-u.ac.jp.
[†] Research Institute for Advanced Science and Technology, Osaka Prefecture University.
[‡] Graduate School of Engineering, Osaka Prefecture University.
[§] Graduate School of Science, Osaka City University.
[∥] Rigaku Corporation.
[⊥] Graduate School of Science, Tohoku University.
[#] Center for Low-Temperature Science, Tohoku University.
[▽] Center for Interdisciplinary Research, Tohoku University.

(1) Day, P. *Philos. Trans. R. Soc. London, Ser. A* **1985**, *145*, 314.
(2) Kurmoo, M.; Graham, A. W.; Day, P.; Coles, S. J.; Hursthouse, M. B.; Caulfield, J. L.; Singleton, J.; Pratt, F. L.; Hayes, W.; Ducasse, L.; Guionneau, P. *J. Am. Chem. Soc.* **1995**, *117*, 12209.
(3) Martin, L.; Turner, S. S.; Day, P.; Mabbs, F. E.; McInnes, E. J. L. *Chem. Commun.* **1997**, 1367.
(4) Ojima, E.; Fujiwara, H.; Kato, K.; Kobayashi, H.; Tanaka, H.; Kobayashi, A.; Tokumoto, M.; Cassoux, P. *J. Am. Chem. Soc.* **1999**, *121*, 5581.
(5) Fujiwara, H.; Fujiwara, E.; Nakazawa, Y.; Narymbetov, B. Z.; Kato, K.; Kobayashi, H.; Kobayashi, A.; Tokumoto, M.; Cassoux, P. *J. Am. Chem. Soc.* **2001**, *123*, 306.

10.1021/ic020143h CCC: $22.00
Published on Web 08/16/2002

2′,5′-diselenafulvalene)$_2$·$FeBr_4$,[6] a ferromagnetic metal based on (BEDT-TTF)$_2$·[$MnCr(C_2O_3)$],[7] and a field-induced ferromagnetic superconductor based on λ-(BETS)$_2$·$FeCl_4$.[8] However, simultaneous appearance of novel magnetism and electrical conductivity in the CT salts as above is not always a result of the interaction between the conducting π electrons and the local d spins involved there. Generally, the π/d interaction is scarcely any or very weak in all the CT salts except for λ-(BETS)$_2$·$FeCl_4$,[9] in which significant π/d interaction, however, begins to occur only at low temperatures.

Under the circumstances it is now desired to urgently search for donor molecules other than BETS, which give new CT salts with magnetic-metal counteranions exhibiting much more increased π/d or π/f interaction, by which unprecedented electrical conducting and/or magnetic properties might come out. Very recently, we synthesized new donor molecules of tetrathiafulvalenothioquione- and tetrathiafulvalenoquinone-1,3-dithiolemethides[10,11] as such candidates. These donor molecules have characteristics of electron-donating ability comparable to that of tetrathiafulvalene to readily produce the corresponding CT salts with magnetic-metal counteranions as well as of binding several magnetic metal salts by coordination with S and O atoms of thiocarbonyl and carbonyl groups residing in their molecules. Indeed, dialkylthio-substituted thiocarbonyl derivatives gave CT salts with $CuCl_4^{2-}$,[11] $FeC1_4^-$,[12] and $FeBr_4^-$ [12] ions and CT complexes coordinated by one $CuBr_2$ molecule.[13] Unfortunately, these CT salts and complexes exhibited low room-temperature electrical conductivities, semiconducting properties, and only very weak π/d interaction. On the other hand, a comparatively high room-temperature electrical conductivity (16 S cm^{-1}) was observed in the plate crystals of a 2:1 CT salt of ethylenedithiotetrathiafulvalenoquinone-1,3-dithiolemethide (**1**) with an $FeBr_4^-$ ion (**1**$_2$·$FeBr_4$), but

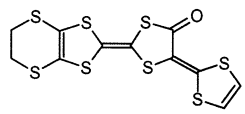

1

its electrical conducting property was still semiconducting and there was no π/d interaction.[14] Now, another crystal phase of **1**$_2$·$FeBr_4$ was obtained as the needle crystals, whose structure is different from that of the plate crystals, and very interestingly exhibited a metallic conducting property and furthermore a ferromagnetic interaction of the d spins of $FeBr_4^-$ ions, although a similar phenomenon has very recently been observed in a 2:1 CT salt of a TTF derivative with an Ni(maleonitriledithiolate)$_2$ ion.[15] The possibility of π/d interaction in **1**$_2$·$FeBr_4$ was discussed on the basis of the comparison of electrical conducting properties with the corresponding nonmagnetic $GaBr_4^-$ salts (**1**$_2$·$GaBr_4$) as well as on the magnetic and ESR results of **1**$_2$·$FeBr_4$.

Experimental Section

Synthesis of 1$_2$·$FeBr_4$ and 1$_2$·$GaBr_4$. The two CT salts were obtained as black-colored needle crystals by the reaction of **1** with $FeBr_3$ or $GaBr_3$ in the following three-phase contact method. Thus, above a solution of **1** (3 mg, 7.3×10^{-3} mmol) in CS_2 (5 mL) was gently placed a CH_3CN solvent (2 mL), and furthermore above the CH_3CN solvent was gently placed a solution of $FeBr_3$ (22 mg, 7.3×10^{-2} mmol) or $GaBr_3$ (23 mg, 7.3×10^{-2} mmol) in CH_3CN (5 mL). The three-phase solution was kept at room temperature. After about 1 week the needle crystals of **1**$_2$·$FeBr_4$ (mp >300 °C) and **1**$_2$·$GaBr_4$ (mp >300 °C) appeared at the interface between the upper two phases. Their elemental analyses gave satisfactory results. Calcd for **1**$_2$·$FeBr_4$ ($C_{22}H_{12}O_2S_{16}FeBr_4$): C, 22.08; H, 1.01. Found: C, 21.89; H, 0.85. Calcd for **1**$_2$·$GaBr_4$ ($C_{22}H_{12}O_2S_{16}GaBr_4$): C, 21.82; H, 1.00. Found: C, 21.82; H, 1.02.

X-ray Data Collection, Structure Solution, and Refinement. The X-ray diffraction data were collected at 113 K for the needle crystals of **1**$_2$·$FeBr_4$ and **1**$_2$·$GaBr_4$ on a Rigaku RAXIS-RAPID imaging plate diffractometer with graphite-monochromated Mo Kα radiation ($\lambda = 0.71069$ Å). Table 1 shows the crystallographic data for the two crystals. The structures were solved by direct methods (SIR92,[16] SIR97,[17] and DIRDIF94[18]) and refined on F_o^2 with full-matrix least-squares analysis. Calculated positions of the hydrogen atoms [d(C−H) = 0.95 Å] were included in the final calculations. All the calculations were performed by using the teXsan crystallographic software package of the Molecular Structure Corporation.[19] For **1**$_2$·$FeBr_4$ the final cycle of least-squares refinement on F_o^2 for 3136 data and 287 parameters converged to wR2(F_o^2) = 0.217 for all the data and to R1 = 0.098 for 3084 data with $I \geq 3.00\sigma(I)$. For **1**$_2$·$GaBr_4$ the final cycle of least-squares refinement on F_o^2 for 3445 data and 287 parameters converged to wR2(F_o^2) = 0.182 for all the data and to R1 = 0.092 for 3241 data with $I \geq 3.00\sigma(I)$.

Electrical Conductivity, Magnetic Susceptibility, and ESR Measurements. Electrical conductivity was measured on each of the needle crystals of **1**$_2$·$FeBr_4$ and **1**$_2$·$GaBr_4$ using a four-probe

(6) Enoki, T.; Umeyama, T.; Miyazaki, A.; Nishikawa, H.; Ikemoto, I.; Kikuchi, K. *Phys. Rev. Lett.* **1998**, *81*, 3719.
(7) Coronado, E.; Galán-Mascarós, J. R.; Gómez-Garcia, C. J.; Laukhin, V. *Nature* **2000**, *408*, 447.
(8) Uji, S.; Shinagawa, H.; Terashima, T.; Yakabe, T.; Terai, Y.; Tokumoto, M.; Kobayashi, A.; Tanaka, H.; Kobayashi, H. *Nature* **2001**, *410*, 908.
(9) Kobayashi, H.; Tomita, H.; Naito, T.; Kobayashi, A.; Sakai, F.; Watanabe, T.; Cassoux, P. *J. Am. Chem. Soc.* **1996**, *118*, 368.
(10) Iwamatsu, M.; Kominami, T.; Ueda, K.; Sugimoto, T.; Fujita, H.; Adachi, T. *Chem. Lett.* **1999**, 329.
(11) Iwamatsu, M.; Kominami, T.; Ueda, K.; Sugimoto, T.; Tada, T.; Nishimura, K−i.; Adachi, T.; Fujita, H.; Guo, F.; Yokogawa, S.; Yoshino, H.; Murata, K.; Shiro, M. *J. Mater. Chem.* **2001**, *11*, 385.
(12) Kominami, T.; Matsumoto, T.; Ueda, K.; Sugimoto, T.; Murata, K.; Shiro, M.; Fujita, H. *J. Mater. Chem.* **2001**, *11*, 2089.
(13) Iwamatsu, M.; Kominami, T.; Ueda, K.; Sugimoto, T.; Adachi, T.; Fujita, H.; Yoshino, H.; Mizuno, Y.; Murata, K.; Shiro, M. *Inorg. Chem.* **2000**, *39*, 3810.
(14) Matsumoto, T.; Kominami, T.; Ueda, K.; Sugimoto, T.; Tada, T.; Yoshino, H.; Murata, K.; Shiro, M.; Negishi, E.-i.; Matsui, H.; Toyota, N.; Endo, S.; Takahashi, K. *J. Solid State Chem.*, in press.
(15) Nishijo, J.; Ogura, E.; Yamaura, J.; Miyazaki, A.; Enoki, A.; Takano, T.; Kuwatani, Y.; Iyoda, M. *Solid State Commun.* **2000**, *116*, 661.
(16) Altomare, A.; Burlea, M. C.; Gamalli, M.; Cascarano, M.; Giacovazzo, C.; Guagliardi, A.; Polidre, G. *J. Appl. Crystallogr*. **1994**, *27*, 435.
(17) Altomare, A.; Burlea, M. C.; Gamalli, M.; Cascarano, G. L.; Giacovazzo, C.; Guagliardi, A.; Moliterni, A. G. G.; Polidre, G.; Spagna, R. *J. Appl. Crystallogr*. **1999**, *32*, 115.
(18) Beurskens, P. T.; Admiraal, G.; Beurskens, G.; Bosman, W. P.; de Gelder, D.; Israel, R.; Smith, J. M. M. In *Technical Report of the Crystallography Laboratory*; University of Nijmegen: The Netherlands, 1994.
(19) *TeXsan, Crystal Structure Analysis Package*; Molecular Structure Corporation: Houston, TX, 1985 and 1992.

Table 1. Crystallographic Data for $\mathbf{1}_2$·$FeBr_4$ and $\mathbf{1}_2$·$GaBr_4$

	$\mathbf{1}_2$·$FeBr_4$	$\mathbf{1}_2$·$GaBr_4$
formula	$(C_{11}H_6OS_8)_2$·$FeBr_4$	$(C_{11}H_6OS_8)_2$·$GaBr_4$
M_r	1196.76	1210.63
cryst size (mm)	0.30 × 0.04 × 0.01	0.15 × 0.02 × 0.02
cryst habit	black needle	black needle
cryst syst	triclinic	triclinic
space group	*P*1	*P*1
a (Å)	6.699(1)	6.712(3)
b (Å)	7.092(1)	7.081(4)
c (Å)	19.579(3)	19.442(8)
α (deg)	81.460(9)	80.792(7)
β (deg)	88.397(6)	88.48(1)
γ (deg)	80.859(4)	80.84(1)
cell vol (Å^3)	908.3(3)	900.5(8)
Z	1	1
temp (K)	113	113
ρ (g cm^{-3})	2.188	2.232
$\mu_{MoK\alpha}$ (cm^{-1})	53.90	61.69
θ_{max}	50.5	50.5
voltage, current	60 kV, 90 mA	60 kV, 90 mA
scan type	*ω*	*ω*
unique data	3136	3445
R_{merge}	0.08	0.11
weighting scheme	$1/\sigma^2(F_o^2)$	$1/\sigma^2(F_o^2)$
resid electron dens (min, max) (e Å^{-3})	−1.47, 3.23	0.00, 1.23
no. of params refined	287	287
R1[a]	0.098	0.092
wR2[b]	0.217	0.182

[a] $R1 = (\sum||F_o| - |F_c||)/(\sum|F_o|)$. [b] $wR2 = [\sum w(F_o^2 - F_c^2)^2/\sum w(F_o^2)^2]^{1/2}$.

method in the temperature range 5−300 K. The contact to the electrode was performed with gold paste. The magnetization at different temperatures between 1.8 and 300 K was measured using microcrystals of $\mathbf{1}_2$·$FeBr_4$ under an applied field of 1 kOe with a SQUID magnetometer (MPMS XL, Quantum Design). The magnetic susceptibility (χ_{obs}) was obtained by dividing the magnetization with the applied field used. The paramagnetic susceptibility (χ_p) was obtained by subtracting the diamagnetic contribution calculated by a Pascal method[20] from χ_{obs}. The ESR spectra of the microcrystals of $\mathbf{1}_2$·$FeBr_4$ and $\mathbf{1}_2$·$GaBr_4$ were recorded with a frequency of 9.46672 GHz using a Bruker ESP-300E spectrometer. The *g* value was determined using a gaussmeter.

Results and Discussion

Molecular and Crystal Structures of the Needle Crystals of $\mathbf{1}_2$·$FeBr_4$ and $\mathbf{1}_2$·$GaBr_4$. The needle crystals of $\mathbf{1}_2$·$FeBr_4$ involve two crystallographically independent **1** molecules (**A** and **B**), whose molecular structures are very similar to each other and have in whole fairly high planarity, since the terminal 1,4-dithiacyclohexene and 1,3-dithiole rings in **A** and **B** molecules are twisted by 8.0° and 8.6° to each other, respectively. As seen from the projection down to the *bc* plane in Figure 1a, the **A** and **B** molecules are stacked along the *b* axis with alternation of their molecular axis direction to form a one dimensionally stacked column. Each of the **1**-stacked columns has two slightly different interplanar distances of 3.48 Å between **A** and **B** molecules, and 3.57 Å between **B** and **A′** molecules, which are comparable to "*π*-cloud thickness (3.50 Å)" [21] or slightly longer. Figure 2a and Figure 2b show the overlaps between

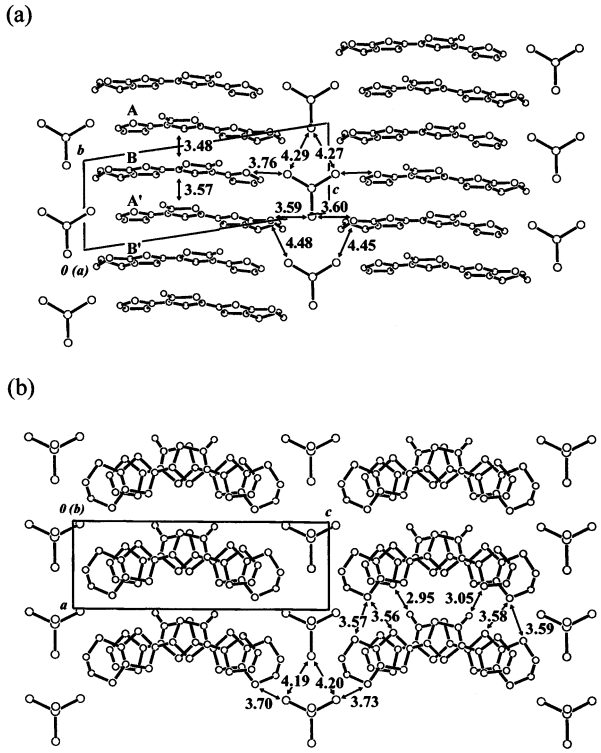

Figure 1. The crystal structure of the needle crystals of $\mathbf{1}_2$·$FeBr_4$: the projections down to the (a) *bc* and (b) *ac* planes.

A and **B** molecules and between **B** and **A′** molecules, respectively. Both overlaps are very similar to each other except that both **1** molecules are only slipped by 0.7 Å in the *a* axis direction and by 0.05 Å in the *c* axis direction. In both contacts an effective overlap occurs between the three five-membered rings of **1** molecules except for the 1,4-dithiacyclohexene rings, i.e., between the skeletal and terminal 1,3-dithiole rings and between the central 1,3-dithiolane-2-thione rings. The HOMO of **1** calculated by the MOPAC method preferentially possesses large AO coefficients on each atom of the skeletal 1,3-dithiole and 1,3-dithiolane-2-thione rings, so that supposedly the overlap between the 1,3-dithiolane-2-thione rings plays an important role in the electron conduction in the needle crystals of $\mathbf{1}_2$·$FeBr_4$. Furthermore, the **1**-stacked columns are aligned along the *a* axis (see Figure 1b). There are several close contacts between the S atoms of **1** molecules in the neighboring columns, and their distances are 2.95−3.59 Å, which are fairly shorter than the sum (3.70 Å) of the van der Waals radii of two S atoms.[21] As a result, a two-dimensional sheet composed of the **1**-stacked columns extends on the *ab* plane, although the $FeBr_4^-$ ion layers intervene between the sheets.

The needle crystal structure of $\mathbf{1}_2$·$GaBr_4$ is almost close to that of $\mathbf{1}_2$·$FeBr_4$. It is a matter of course, since both the $GaBr_4^-$ and $FeBr_4^-$ ions have almost the same tetrahedral-like geometry around the central Ga and Fe atoms, and they have almost the same volume, except that the $GaBr_4^-$ ion is a nonmagnetic ion in contrast to the magnetic $FeBr_4^-$ ion.

(20) König, E. *Landolt-Bornstein, Group II: Atomic and Molecular Physics, Vol. 2, Magnetic Properties of Coordination and Organometallic Transition Metal Compounds*; Springer-Verlag: Berlin, 1966.

(21) Pauling, L. *The Nature of the Chemical Bond*, 3rd ed.; Cornell University Press: Ithaca, New York, 1960.

The interplanar distances between **A**/**B** and **B**/**A′** are 3.50 and 3.54 Å, which are longer and shorter by 0.03 Å than the corresponding values in $\mathbf{1}_2$·$FeBr_4$, respectively. In addition, the side by side contacts between **A**/**A**, **B**/**B**, and **A**/**B** have slightly different distances by 0.01−0.04 Å from those in $\mathbf{1}_2$·$FeBr_4$.

On the other hand, both the $FeBr_4^-$ ion in $\mathbf{1}_2$·$FeBr_4$ and the $GaBr_4^-$ ion in $\mathbf{1}_2$·$GaBr_4$ have slightly distorted-tetrahedral geometry, since the six Br−Fe−Br bond angles (107.4°, 108.3°, 108.3°, 109.3°, 110.4°, and 111.3°) for the $FeBr_4^-$ ion and the six Br−Ga−Br bond angles (108.2°, 108.3°, 109.2°, 109.2°, 109.2°, and 110.3°) for the $GaBr_4^-$ ion are significantly different from each other, although each of the four Fe−Br and Ga−Br bond distances are almost the same (2.31−2.34 and 2.32−2.34 Å). The $FeBr_4^-$ and $GaBr_4^-$ ions intervene between the **1**-stacked columns and are aligned along the *b* axis with the direction of the geometry being completely maintained in a straight manner. There are two slightly different Br−Br contacts with the longer distances of 4.27 and 4.29 Å and 4.30 and 4.32 Å than the sum (3.90 Å) of the van der Waals radii of two Br atoms[21] between the neighboring $FeBr_4^-$ and $GaBr_4^-$ ions in the respective arrays. Furthermore, the $FeBr_4^-$ and $GaBr_4^-$ ion arrays are aligned along the *c* axis. The Br−Br contacts between the neighboring $FeBr_4^-$ and $GaBr_4^-$ ions in the inter-arrays have distances of 4.19 and 4.20 Å for the $FeBr_4^-$ ion and 4.18 and 4.21 Å for the $GaBr_4^-$ ion, respectively. Their Br−Br contact distances in whole become fairly shorter than those in the intra-arrays. As a result the $FeBr_4^-$ ions are arranged to form a square lattice in the *bc* plane, so that the exchange interaction between the d spins of the $FeBr_4^-$ ions are two-dimensional. In addition, several short contacts are seen between the S atoms of **1** molecules and the Br atoms of $FeBr_4^-$ or $GaBr_4^-$ ions. Thus, the contact distances between the S atoms of the 1,3-dithiole rings and the Br atoms of the $FeBr_4^-$ ($GaBr_4^-$) ions and between the S atoms of the 1,4-dithiacyclohexene rings and the Br atoms of the $FeBr_4^-$ ($GaBr_4^-$) ions are 3.76 (3.72) and 3.78 (3.78) and 3.59 (3.57), 3.60 (3.59), 3.73 (3.78), and 3.70 (3.73) Å, respectively, which are in whole shorter than the sum (3.80 Å) of the van der Waals radii of S and Br atoms.[21]

Electrical Conducting Properties. The needle crystals of $\mathbf{1}_2$·$FeBr_4$ and $\mathbf{1}_2$·$GaBr_4$ have the considerable length of ca. 1 mm, but their sectional plane is very narrow (0.05 × 0.2 mm^2 at the largest). Consequently, four probes could only be put on the needle plane, which is most supposed to correspond to the direction of the stacking of **1** molecules, although it was unsuccessful to determine the relationship between the crystal structure and the crystal shape, because the diffractions from the plane perpendicular to the needle plane were too weak to be analyzed. Figure 3 shows temperature dependences of the electrical conductivities (σ's, reciprocal of electrical resistivities (ρ's)) of $\mathbf{1}_2$·$FeBr_4$ and $\mathbf{1}_2$·$GaBr_4$ in the temperature range 5−300 K. The σ's at 300 K were comparatively high: 4.6 S cm^{-1} for $\mathbf{1}_2$·$FeBr_4$ and 2.1 S cm^{-1} for $\mathbf{1}_2$·$GaBr_4$. As seen from the temperature dependences of ρ's in the temperature ranges 300−20 K (Figure 3a) and 20−5 K (Figure 3b), for both crystals the ρ's gradually decreased as the temperature was lowered from 300 K, and the decrease in ρ continued till ca. 170 K. Such a temperature dependence of ρ is reminiscent of metal-like electrical conducting behavior. However, below ca. 170 K the ρ's reversely increased with lowering temperature and the gradual increase in ρ continued till 5 K, indicating that a semiconducting behavior is preferential in the temperature range of ∼170−5 K for both crystals. Figure 3c shows the plots of $\ln(1/\rho)$ vs $1/T$ in the overall temperature range measured. A slope of the straight line obtained by such a plot corresponds to an activation energy (E_a) for the electron conduction. Nevertheless, as is obvious from Figure 3c, the plots of $\ln(1/\rho)$ vs $1/T$ gave a slightly curved line in the temperature range 300−5 K for both cases. The slope (i.e., E_a) gradually decreased with lowering temperature. For $\mathbf{1}_2$·$FeBr_4$ the E_a's were 9.7 meV in the higher temperature range (100−20 K) and 4.2 meV in the lower temperature range (10−5 K). The corresponding values in $\mathbf{1}_2$·$GaBr_4$ were 10.1 and 4.0 meV, respectively. These results indicate that both $\mathbf{1}_2$·$FeBr_4$ and $\mathbf{1}_2$·$GaBr_4$ are undoubtedly semiconductors, but can actually be regarded as semi-metal or metal-like in view of very small E_a's. In addition, it should be noted that there is almost no change in the electrical conducting properties between $\mathbf{1}_2$·$FeBr_4$ and $\mathbf{1}_2$·$GaBr_4$, suggesting that the magnetic moment of $FeBr_4^-$ d spins exerts no influence on the π electron conduction due to the **1**-stacked columns as far as one looks at the electrical conducting results till 5 K.

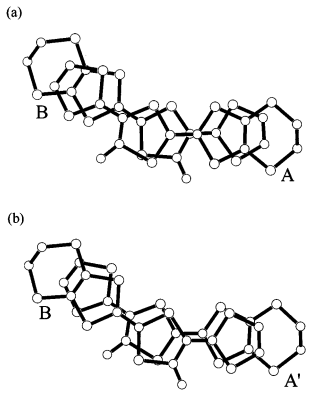

Figure 2. The contacts of two neighboring **1** molecules (**A** and **B**) in the needle crystals of $\mathbf{1}_2$·$FeBr_4$: (a) **A**/**B** and (b) **B**/**A′** contacts.

ESR Spectra. The ESR spectra of $\mathbf{1}_2$·$FeBr_4$ and $\mathbf{1}_2$·$GaBr_4$ were measured using their needle microcrystals. The ESR spectrum of $\mathbf{1}_2$·$FeBr_4$ at 300 K showed only one broad signal with a very large peak-to-peak width (ΔH_{pp}) of 885 Oe at g = 2.069. Since the observed g and ΔH_{pp} values are comparable to those (2.050 and 568 Oe) of NEt_4·$FeBr_4$, this signal can be assigned to the d spins of $FeBr_4^-$ ions. In addition, the signal due to the spins of conducting π electrons on the **1**-stacked columns might be also hidden in the signal observed. However, it is not possible, judging from the ESR result of $\mathbf{1}_2$·$GaBr_4$, in which no signal was observed as a result of marked broadening at 300 K, although one broad signal of ΔH_{pp} = 33 Oe with very weak intensity began to appear at g = 2.006 at around 40 K and the intensity gradually increased with lowering temperature from 40 K. The temperature dependence in the ESR spectrum of $\mathbf{1}_2$·

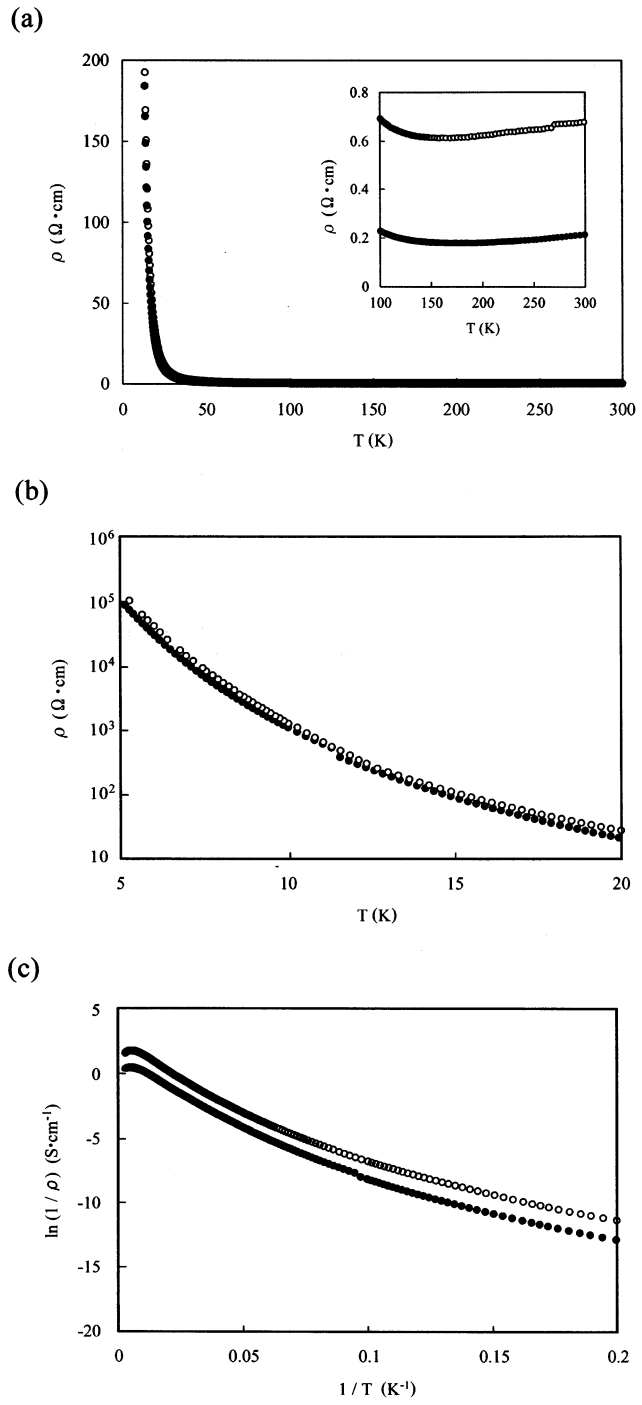

Figure 3. Temperature dependences of ρ for the needle crystals of (●) $\mathbf{1}_2$·$FeBr_4$ and (○) $\mathbf{1}_2$·$GaBr_4$ in the temperature range (a) 20−300 K and (b) 5−20 K. (c) Plots of ln(1/ρ) vs 1/T for the needle crystals of (●) $\mathbf{1}_2$·$FeBr_4$ and (○) $\mathbf{1}_2$·$GaBr_4$ in the temperature range 5−300 K.

$FeBr_4$ was also investigated in the temperature range 3−300 K. In the whole temperature range a signal shape was not changed at all, but g and ΔH_{pp} values showed marked temperature dependence. The results are shown in Figure 4a and Figure 4b, respectively. The g value of 2.069 at 300 K increased with lowering temperature and reached 2.173 at 3 K. Especially, the increase below ca. 15 K was very abrupt. A similar tendency was also observed in the temperature dependence of ΔH_{pp}. The value was almost constant (about 890 Oe) between 300 and ca. 100 K, but

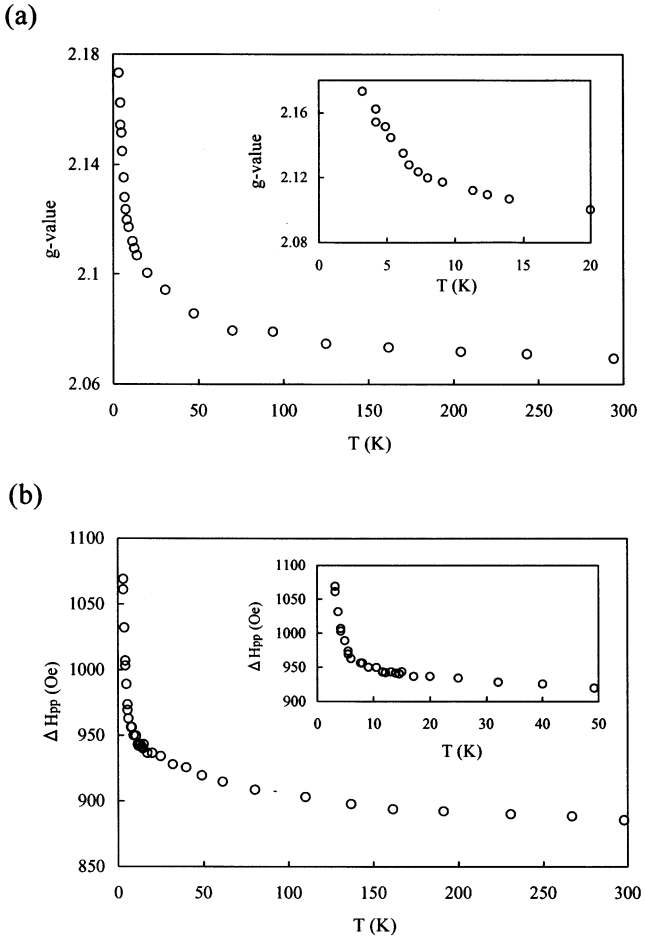

Figure 4. Temperature dependences of (a) the g value and (b) ΔH_{pp} of the ESR signal for the needle crystals of $\mathbf{1}_2$·$FeBr_4$ in the temperature range 3−300 K.

below ca. 100 K it increased with lowering temperature. An abrupt increase began to occur at ca. 15 K and continued till 3 K, where ΔH_{pp} was 1069 Oe. This kind of temperature dependence of g and ΔH_{pp} values is very similar to that observed in a low-dimensional spin system of magnetic metal salts in which short-range spin ordering occurs at low temperature.[22,23] Thus, it is most probable that the d spins of $FeBr_4^-$ ions have a tendency of completing short-range ordering in the two-dimensional square lattice at low temperature.

Magnetic Properties. The temperature dependence of the product of χ_p with T ($\chi_p T$) for the needle microcrystals of $\mathbf{1}_2$·$FeBr_4$ is shown in Figure 5a, in which the $\chi_p T$ gradually decreased as the temperature was cooled down from 300 K, and such a trend continued till ca. 15 K. The temperature dependence of χ_p in this temperature range of ca. 25−300 K was well reproduced with an equation of $\chi_p = C/(T - \theta) + \chi_\pi$, where C is the Curie constant and θ is the Weiss temperature, and these values are related to the d spins of $FeBr_4^-$ ions, while χ_π is a temperature-independent χ_p related to the π conducting electrons on the **1**-stacked columns. Since the electrical conduction is actually metallic in the present case, χ_π can be assigned to the χ_p due to the Pauli

(22) Oshima, K.; Okuda, K.; Date, M. *J. Phys. Soc. Jpn.* **1976**, *41*, 475.
(23) Mori, H. *Prog. Theor. Phys.* **1963**, *30*, 578.

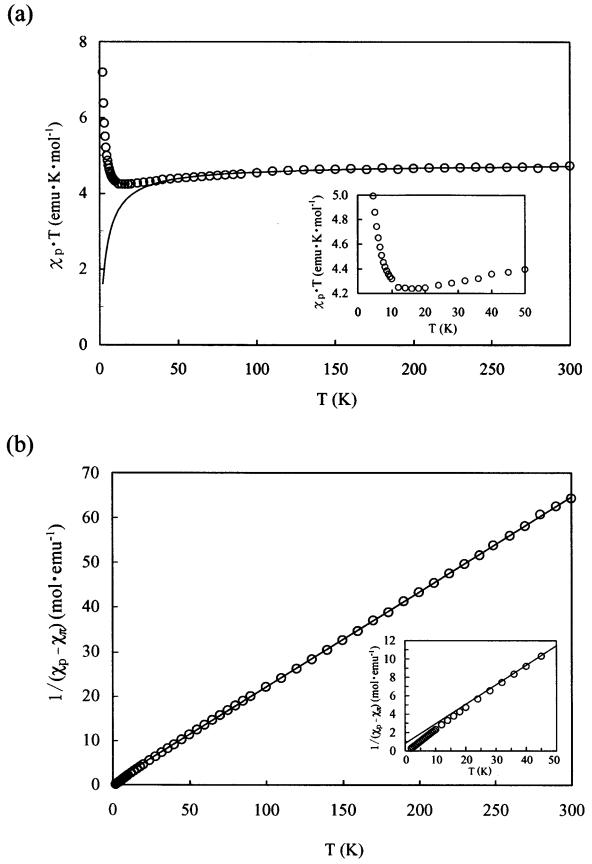

Figure 5. Temperature dependences of (a) χ_pT and (b) $1/(\chi_p - \chi_\pi)$ for the needle crystals of $\mathbf{1}_2$·$FeBr_4$ in the temperature range 1.8−300 K. The solid line in plot a and the straight line in plot b were obtained by adding $C = 4.71$, $\theta = -3.9$, and $\chi_\pi = 2.0 \times 10^{-4}$ to the equations of $\chi_p = C/(T - \theta) + \chi_\pi$ and $1/(\chi_p - \chi_\pi) = (1/C)T - (1/C)\theta$, respectively.

paramagnetism. The best fitted values are $C = 4.71$ emu K mol^{-1}, $\theta = -3.9$ K, and $\chi_\pi = 2.0 \times 10^{-4}$ emu mol^{-1}, respectively. The C obtained is very close to the value (4.68 emu K mol^{-1}) calculated as an Fe(III) d spin entity with $S = {}^5/_2$ and $g = 2.069$. The θ value is very small and negative, indicating that very weak and antiferromagnetic interaction preferentially occurs between the d spins of $FeBr_4^-$ ions. The χ_π is similar to those observed in several organic metallic conductors.[2]

Nevertheless, below ca. 15 K the χ_pT sharply increased with lowering temperature, suggesting the occurrence of ferromagnetic interaction between the Fe(III) d spins. As seen from the temperature dependence of the reciprocal of $(\chi_p - \chi_\pi)$ $(1/(\chi_p - \chi_\pi))$ in Figure 5b, in the temperature range of ca. 25−300 K such a straight line was obtained that crossed the temperature axis at ca. −3.9 K, while, in the temperature region lower than ca. 20 K, the $1/(\chi_p - \chi_\pi)$ values began to come off from the straight line as above and monotonically decreased with lowering temperature to finally cross the temperature axis at +0.87 K. This temperature corresponds to θ below ca. 20 K, indicating that the $FeBr_4^-$ d spins are subject to weak and ferromagnetic interaction. The slope of the straight line in the higher temperature region corresponds to $1/C$ ($C = 4.71$), but below ca. 20 K the slope ($1/C$; $C = 3.98$) became steeper. Thus, the C value in the lower temperature region decreased by ca. 15% compared with that

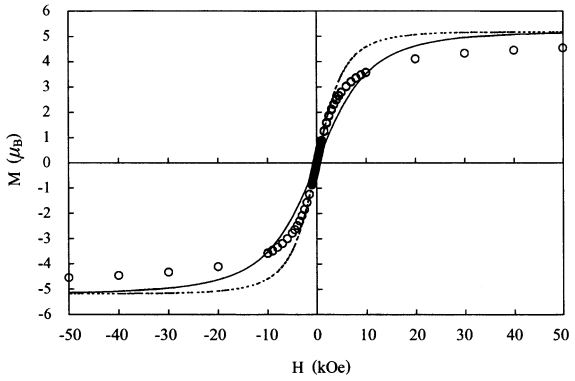

Figure 6. Magnetization (M) curve for the needle crystals of $\mathbf{1}_2$·$FeBr_4$ in the field range of ±50 kOe at 1.8 K. The Brillouin functions with $S = {}^5/_2$ and $\theta = 0$ K (−) and with $S = {}^5/_2$ and $\theta = +0.87$ K (- - -) at 1.8 K are also depicted.

in the higher temperature region. Since C is formulated by $Ng^2\mu_B2S(S + 1)$ (N, spin amount (usually Avogadro's number, 6×10^{23} per mol); g, g value; μ_B, Bohr magneton; S, spin quantum number), the decrease in C is caused by decreased N, g, and/or S. As shown in Figure 4a, the g value increases with lowering temperature, and it is hardly probable that some of 6×10^{23} Fe(III) ($S = {}^5/_2$) d spins per mole of $\mathbf{1}_2$·$FeBr_4$ contributing to the magnetism in the higher temperature region has no participation in the lower temperature region, so that the g and N can be excluded from the above cause.

Accordingly, there remains as a possible cause that the S value of the Fe d spin becomes smaller than ${}^5/_2$ by some geometrical change around the Fe atom in the $FeBr_4^-$ ion or by significant antiferromagnetic interaction of the π spins on the **1**-stacked columns with the Fe(III) ($S = {}^5/_2$) d spins. Now, the magnetization (M) curve was measured in the applied field (H) range of ±50 kOe at 1.8 K, the lowest temperature used in our experiment (see Figure 6). The sigmoidal curve without a hysteresis (a coercive force <7 Oe) was obtained, in which the M value under $H = \pm 50$ kOe is ±25350 emu mol^{-1} (±4.39 μ_B) and tends to further increase with increasing H from ±50 kOe. The computational simulation predicts that the saturation in M will occur under under $H =$ ca. ±300 kOe, and the value amounts to ± 28900 emu mol^{-1} (±5.00 μ_B), which is very close to that obtained by 6×10^{23} Fe(III) ($S = {}^5/_2$) spins per mole of $\mathbf{1}_2$·$FeBr_4$. This result undoubtedly excludes the possibility of the decreased S state from ${}^5/_2$ in the Fe(III) d spin.

The observed M curve was compared with two related Brillouin functions with $S = {}^5/_2$ and $\theta = 0$ K, and with $S = {}^5/_2$ and $\theta = +0.87$ K at 1.8 K, which are also depicted in Figure 6. In the H range lower than ca. 10 kOe the observed M's are larger than those in the Brillouin function with $\theta = 0$ K at each H. However, the observed M curve shows very good fit to the Brillouin function with $\theta = +0.87$ K in the H field lower than ca. 1 kOe, but above 1 kOe both of the curves are separated out from each other and the observed curve reaches a saturation more slowly than the theoretical one. The cause of the slower saturation behavior in the observed M curve can be reasonably explained by considering that at low temperature the π spins in the **1**-stacked

column participate in the antiferromagnetic interaction with the Fe(III) d spins to eventually make the interaction between the neighboring Fe(III) d spins ferromagnetic. It is obvious that in the spin-interacting system as above the magnetic moments of Fe(III) d spins are forced into slower saturation by the presence of the magnetic moment of the π spins in the reverse direction.

Concluding Remarks

Both of the needle crystals of $\mathbf{1}_2$·$FeBr_4$ and $\mathbf{1}_2$·$GaBr_4$ exhibited almost the same electrical conducting properties, which were metallic between ca. 170 and 300 K, while semiconducting with very small activation energies of 4−10 meV between 5 and ca. 170 K. These results clearly suggest that the magnetic moments due to d spins of $FeBr_4^-$ ions exert no influence on the conducting π electrons on the **1**-stacked columns in the whole temperature range 5−300 K. As the main cause it is conceivable that there was scarcely any contact between the **1** molecule and the $FeBr_4^-$ ion even at low temperatures, as seen in λ-$(BETS)_2$·$FeCl_4$ with very close contact between one Se atom of the BETS molecule and one Cl atom of the $FeCl_4^-$ ion.[9] One promising method to bring about significant S···Br contact is an internal application of high pressure to the needle crystals of $\mathbf{1}_2$·$FeBr_4$. It might be possible that not only is the metallic conducting property maintained till low temperatures but the contact between the **1** molecule and the $FeBr_4^-$ ion also increases by their mutual rearrangement, giving rise to significant π/d interaction at comparatively high temperatures. We are now performing a high-pressure electrical conductivity measurement on the needle crystals of $\mathbf{1}_2$·$FeBr_4$ and $\mathbf{1}_2$·$GaBr_4$.

Nevertheless, it is not adequate to rule out the possibility of some interaction between the π electrons of **1** molecules and the d spins of $FeBr_4^-$ ions, from the unusual magnetic results of $\mathbf{1}_2$·$FeBr_4$ on the transition of antiferromagnetic to ferromagnetic interactions of the d spins of $FeBr_4^-$ ions at ca. 15 K and on the abrupt increase of g and ΔH_{pp} values in the ESR spectrum below ca. 15 K. In general, it is very difficult to understand a drastic change from antiferromagnetic to ferromagnetic by only the spin exchange interaction between the d spins of $FeBr_4^-$ ions, which have very similar arrangements to each other in both the intra- and inter-arrays (see Figure 1a,b). It is rather reasonable to consider some participation of the π spins of **1** molecules for the ferromagnetic interaction between the $FeBr_4^-$ d spins. Thus, in the temperature region higher than ca. 15 K the d spins of $FeBr_4^-$ ions directly interact with each other in a very weak and antiferromagnetic manner, and the π electrons on the **1**-stacked columns preferentially contribute to the metallic conduction. There is not any interaction between both of the electrons, while, below ca. 15 K, the electrical resistivity sharply increases, accompanied with strong localization of the π conducting electrons of **1** molecules. As a result, it might happen that the π electron spins localized on the **1**-stacked columns participate in the exchange interaction between the $FeBr_4^-$ d spins and that such an indirect exchange interaction becomes ferromagnetic by aid of the π electron spins residing on the S atoms of a 1,3-dithiole ring or an ethylenedithio group in a **1** molecule. As supposed by marked increase in g and ΔH_{pp} values below ca. 5 K, the ferromagnetic interaction becomes stronger and might finally be converted to ferromagnetic ordering below 1 K. However, such a symptom could not be recognized by the $M-H$ measurement measured at 1.8 K. To confirm whether the ferromagnetic ordering can occur or not, it is necessary to perform $M-H$ and $M-T$ measurements at a temperature lower than 1 K.

Acknowledgment. This work was supported by a Grant-in-Aid for Scientific Research on Priority Areas (B) (No. 11224209) from the Ministry of Education, Culture, Sports, Science, and Technology, Japan. We thank Dr. H. Fujiwara and Prof. H. Kobayashi (Institute for Molecular Science) for ESR measurement and Dr. M. Mito and Prof. Takeda (Kyushu University) for SQUID measurement under weak magnetic field.

Supporting Information Available: Tables listing atomic positional parameters, bond lengths, and bond angles for the needle crystals of $\mathbf{1}_2$·$FeBr_4$ and $\mathbf{1}_2$·$GaBr_4$. Crystallographic data in CIF format. This material is available free of charge via the Internet at http://pubs.acs.org.

IC020143H